© 2023 The Authors. Published by the British Institute of Radiology under the terms of the Creative Commons Attribution-NonCommercial 4.0 Unported License http://creativecommons.org/licenses/by-nc/4.0/, which permits unrestricted non-commercial reuse, provided the original author and source are credited.

birpublications.org/dmfr

RESEARCH ARTICLE

Three-dimensional mapping of the greater palatine artery location and physiology

¹Baiyan Qi, ²Reza Khazeinezhad, ²Ali Hariri, ¹Wonjun Yim, ³Zhicheng Jin, ³Lekshmi Sasi, ⁴Casey Chen and ^{1,3,5}Jesse V. Jokerst

¹Materials Science and Engineering Program, University of California San Diego, La Jolla, California, United States; ²StyloSonic LLC, Lake Forest, California, United States; ³Department of Nanoengineering, University of California San Diego, La Jolla, California, United States; ⁴Herman Ostrow School of Dentistry, University of Southern California, Los Angeles, California, United States; ⁵Department of Radiology, University of California San Diego, La Jolla, California, United States

Objective: To develop a novel technique for localizing and reconstructing the greater palatine artery (GPA) using three-dimensional (3D) technology.

Methods: A miniaturized intraoral ultrasound transducer was used to imaging landmarks including the GPA, gingival margin (GM), and palatal masticatory mucosa (PMM). A 5-mm-thick solid hydrogel couplant was integrated to replace traditional ultrasound gel and avoid bubbles when moving the transducer.

Results: A panorama image provided the relative localization of landmarks including the GPA, PMM, and hard palate. Short- and long-axis imaging of GPA was performed in five subjects including 3D mapping of GPA branches and surrounding tissues in a volume of 10 mm \times 8 mm \times 10 mm. Full-mouth Doppler imaging was also demonstrated on both the dorsal and ventral tongue as well as buccal mucosa and sublingual region on two subjects.

Conclusions: This study can measure the vertical distance from the GM to the GPA and depth from PMM to GPA and visualize the GPA localization in a 3D manner, which is critical to evaluate the available volume of palatal donor tissues and avoid sectioning of GPA during surgical harvesting of the tissues. Finally, the transducer's small size facilitates full-mouth Doppler imaging with the potential to improve the assessment, diagnosis, and management of oral mucosa.

Dentomaxillofacial Radiology (2023) 52, 20230066. doi: 10.1259/dmfr.20230066

Cite this article as: Qi B, Khazeinezhad R, Hariri A, Yim W, Jin Z, Sasi L, et al. Three-dimensional mapping of the greater palatine artery location and physiology. *Dentomaxillofac Radiol* (2023) 10.1259/dmfr.20230066.

Keywords: periodontitis; tissue grafts; palate; Doppler ultrasound; ultrasonography

Introduction

The PMM is the most common donor site in free softtissue graft for gingival recession treatment¹ including free gingival grafts^{2,3} and subepithelial connective tissue graft.^{4,5} Despite the high success rate of PMM grafting surgeries, several cases have shown that the GPA and its major branches can be dissected due to an inability to accurately locate the GPA. This in turn leads to excessive bleeding.⁶⁻⁹ Therefore, several studies have examined the position of the GPA relative to other landmarks to provide guidance for harvesting PMM soft tissues.^{10–18}

In 2006, Monnet-Corti et al assumed the distance from the GPA to the GM of the canine and the second molar to be 12.07 ± 2.9 mm and 14.7 ± 2.9 mm, respectively, based on measurements done on cast impressions. In 2019, Tavelli et al summarized a series of cadaveric studies that investigated further anatomical details of the GPA in a systematic review. In The distance between the GPA to the teeth gradually

Correspondence to: Jesse V. Jokerst, E-mail: jjokerst@ucsd.edu; Casey Chen, E-mail: ccchen@usc.edu

Received 08 February 2023; revised 01 May 2023; accepted 01 May 2023; published online 24 October 2023

reduces from the second molar region (13.9 \pm 1 mm) toward the canine region (9.9 \pm 2.9 mm).

While these works analyzed the average position of GPA, the distribution of GPA branches in each individual varies. ^{19,20} Reiser et al suggested that the shape of palatal vault could influence the location of the GPA. ¹⁴ Fu et al also reported that the PMM thickness and the large palatal vault curvature could make it difficult for clinicians to precisely estimate the location of GPA. ¹⁵

Therefore, non-invasive methods to locate the GPA and measure the PMM thickness of individual subjects are required to minimize the risk of GPA injury associated with graft procedures. In 2008, Song et al measured the thickness of posterior PMM by computed tomography (CT) in 100 adults. In 2018, Hilgenfeld et al detected the GPA via magnetic resonance imaging (MRI). However, the limitations of these techniques include the ionizing radiation seen in CT, and the expense and long turnaround times of MRI.

One promising alternative to these techniques is ultrasound imaging. Acoustic imaging offers real-time and non-ionizing imaging of soft tissue as well as the surfaces of hard tissue. We and others have used ultrasound to estimate clinical attachment loss²¹ and periodontal probing depth,²² diagnose maxillary fractures, perform guided nerve blocks,²³ evaluate intraosseous lesions,²³ and many other applications.^{24,25}

More recently, Sampietro-Martínez et al²⁶ and Lee et al²⁷ used ultrasound imaging to determine the position and course of the GPA and then evaluate the thickness of the PMM. These results collectively underscore the value of ultrasonography in GPA measurement. However, both of these works are limited to twodimensional (2D) imaging, and the direction of imaging is perpendicular to the direction of PMM harvesting. The distance from the GPA to the teeth and the depth located in the PMM varies from anterior region to posterior region, 10 and thus 3D imaging of the PMM and GPA will provide complete distribution information on the GPA and its branches. Such imaging data will ultimately minimize or remove the risk of GPA damage and help determine the volume of the available PMM donor tissue.

Here, we report for the first time 3D maps of the GPA course relative to the PMM surface via ultrasound imaging with a miniaturized intraoral transducer. We also report solid acoustic couplants integrated into the transducer scan head to remove the need for acoustic coupling gel. The small size of the transducer facilitates both short axis and long axis views of the GPA. The GPA localization results may have value in treatment planning for free soft-tissue graft as well as other periodontal plastic surgeries in the PMM.²⁸ Finally, we show that the miniaturized intraoral transducer can record physiological details including pulse rate via fullmouth Doppler imaging of the tongue, buccal mucosa,

and sublingual regions, which may have potential in the diagnosis of oral cancer.²⁹

Methods and materials

Equipment

A linear array transducer was used to scan the GPA image slices (Figure 1a). The transducer SS-19-128 is a customized side-facing transducer from StyloSonic (Lake Forest, USA) with a center frequency of 19 MHz and 128 transducer elements.³⁰ The size of the transducer is $10 \times 18 \,\mathrm{mm}$ to access the full oral cavity.³⁰ Two commercial transducers L35-16vX (Verasonics, Inc., Kirkland, USA) and CL15-7 (Philips, USAd) were also included (Fig. S1). A data acquisition (DAQ) system (Vantage 256, Verasonics, Inc., Kirkland, USA) was connected to transducers to provide power supply and signal processing by sampling the radiofrequency data from each transducer channel. The DAO system supports a frequency range of 2 to 42 MHz; 14-bit A/D converters with a programmable sample rate up to 62.5 MHz and can image up to 100,000 frames/second.

Human subjects recruitment

This study involved seven healthy human subjects (four males and three females) with a mean age of 28.7 ± 4.9 years old with good oral hygiene. The study protocol (project 170912) was approved by the UCSD Institutional Review Boards. All subjects provided informed consent.

Resolution phantom

A tungsten wire of a 0.001-inch diameter was used to characterize the imaging resolution of ultrasound transducers. The tungsten wire was put in water 1 cm deep from the transducer surface. The axial and lateral resolutions of ultrasound transducers were characterized using a point spread function as described.³¹

Periodontal ultrasonography

Subjects were seated by side of the ultrasound equipment and imaged with oral transducers by an ultrasound researcher (B.Q.) who has four-year experience in operating the ultrasound transducer and analyzing ultrasound images. Our previous works have suggested that the periodontal ultrasound imaging is reproducible for different examiners by investigating the interexaminer bias between a clinician without prior ultrasound experience, and ultrasound researchers with different years of experience.^{21,32} A 5-mm-thick solid hydrogel pad was placed on the transducer for ultrasound coupling. The hydrogel was held in place with a disposable sterile adhesive (Tegaderm; 3M Minneapolis, USA) that was changed between each subject. Real-time 2D cross-sectional B-mode and Color Doppler imaging^{33,34} was performed by manually positioning the transducer in the short- and long-axis along the PMM for the GPA measurement on five subjects. For the dorsal

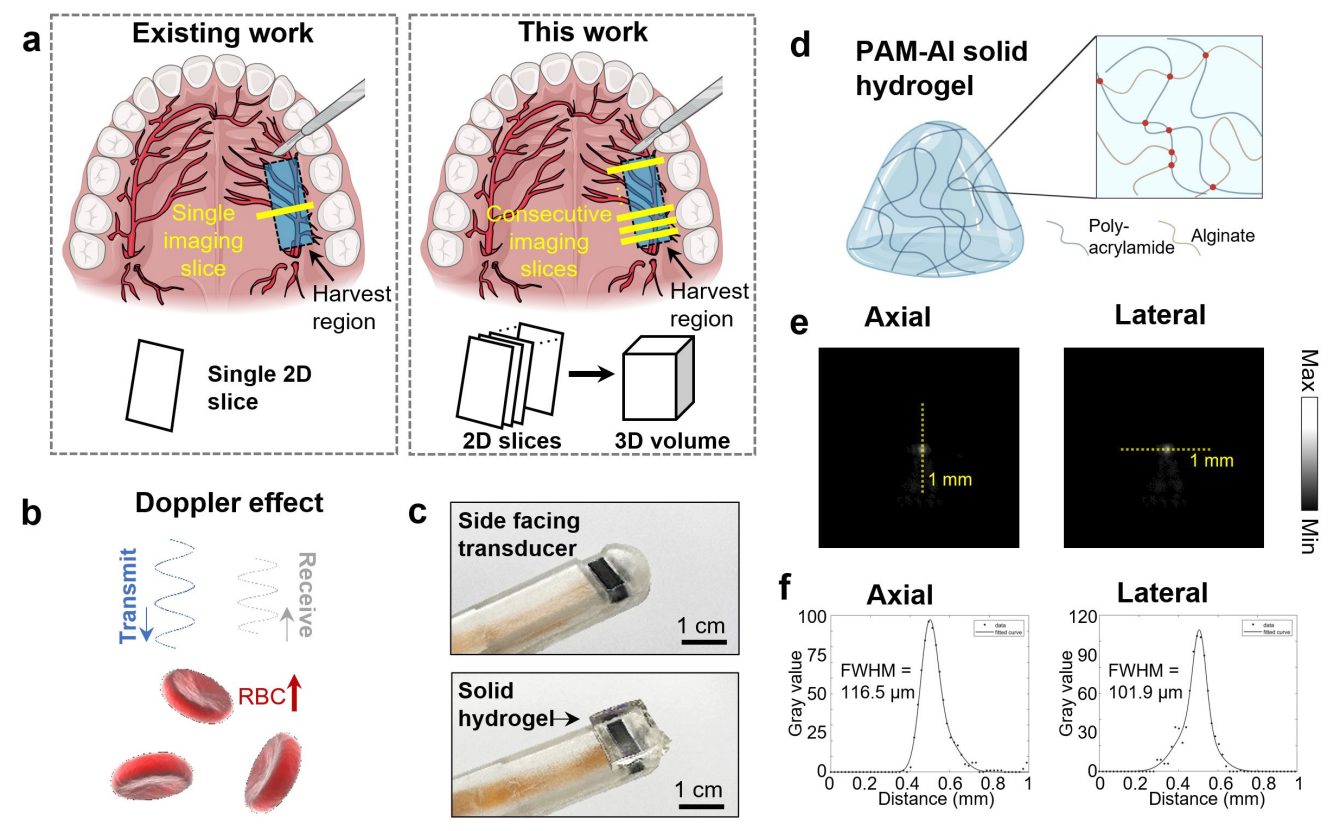


Figure 1 Overview of the 3D GPA measurement. (a) Comparison between existing 2D imaging and the proposed 3D imaging of the GPA. The GPA and its branches contribute to the blood supply of the hard and soft palate. (b) The transducer emitted and received the ultrasound signals scattered by the red blood cells (RBC) thus leading to Doppler effects. The side-facing transducer (c, top) was covered with a polymeric solid couplant material (c, bottom) that was sealed in place with a sterile plastic adhesive; the couplant was prepared from polyacrylamide (d). The resolution of the device was evaluated in both axial and lateral dimensions by imaging a metallic wire (e) and creating line profiles (f). GPA: greater palatine artery. FWHM: full width half maximum.

and ventral tongue, buccal mucosa, and sublingual region, the transducer was positioned along the short axis on two subjects. Blood flow velocity spectrum of the GPA was decoded by the DAQ system³⁵ on subject #1. The principle of detecting ultrasound Doppler signals was presented in Figure 1b.

Polyacrylamide (PAM)- alginate (AI) hydrogel

The couplant was based on alginic acid sodium salt from brown algae (medium viscosity), acrylamide (> 99%), N, N, N', N'-tetramethyl-ethylenediamine (TEMED, > 99%), N, N'-methylenebisacrylamide (MBAA, >99%), ammonium persulfate (APS, 98%). All the above chemicals were purchased from Sigma-Aldrich and used without any further purification. PAM-Al hydrogels were synthesized by the free radical polymerization of acrylamide and ionic crosslinking of alginate.36,37 Typically, 600 mg of alginate sodium salt was dissolved in 40ml of PBS (pH 6.4) under generous stirring at 700 rpm for 1h at 40°C. Then, 4.8 g of acrylamide, 33 mg of MBAA, 36µL of TEMED, and 12mg of APS were added to the homogenous alginate solution for 30 min under the generous stirring at 700 rpm at room temperature. The mixture was poured to a glass petri dish followed by polymerization at 60°C for 0.5h. After the polymerization, PAM-Al hydrogel was removed from the petri dish and washed with distilled water for future use (Figure 1c and d).

Panorama image stitching

The transducer was manually moved from the center of mouth to tooth #15 (2nd molar) at a uniform speed to collect real-time imaging video from GPA to the tooth surface. Then, different frames were extracted from the video and manually stitched one a panorama image by aligning the landmarks (*i.e.*, GPA, PMM surface, and gingiva, etc.) between the adjacent frames. The second frame was adapted 50% transparent to align with the front frame.

3d mapping of GPA

For subject 1, 15 short-axis color Doppler imaging slices along the long axis were collected to reconstruct a 3D map of GPA branches in a volume of $10 \times 8 \text{ mm} \times 10 \text{ mm}$. The Doppler-only 3D mapping was reconstructed by Amira.³⁸ 3D mapping that combines Doppler signals and B-mode was reconstructed by ImageJ.³⁹

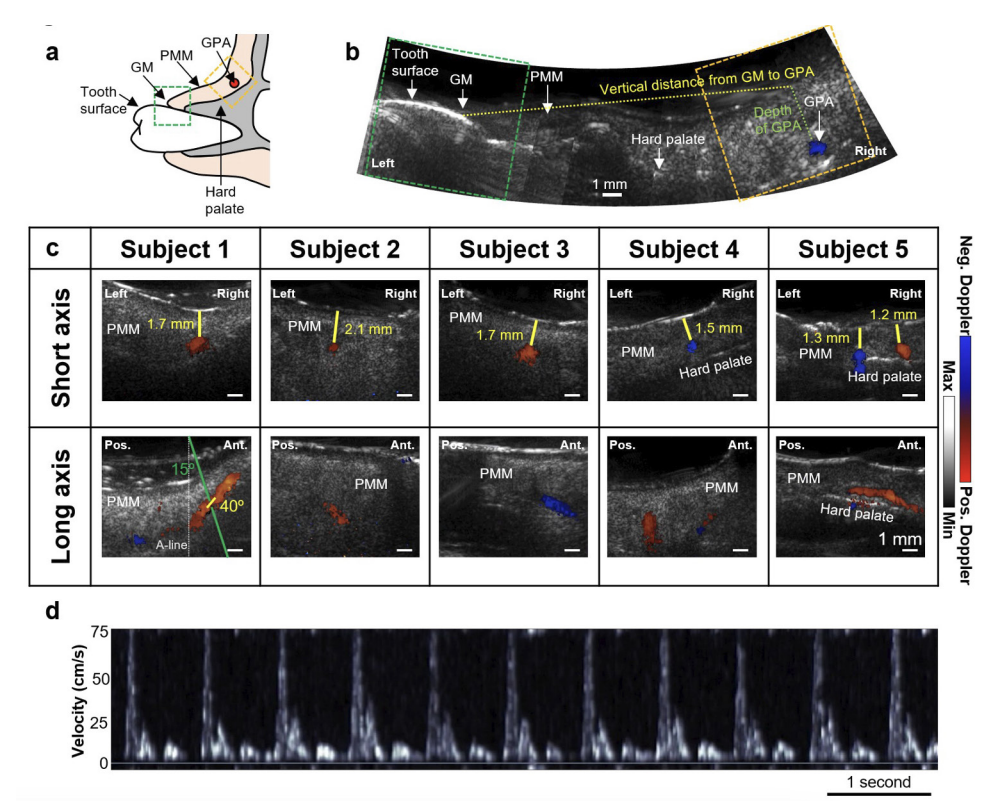


Figure 2 GPA imaging of healthy subjects with SS-19–128. (a and b) Schematic and panoramic image of the oral anatomy including gingival margin (GM), palatal masticatory mucosa (PMM), hard palate, and greater palatine artery (GPA). Depth of GPA from the PMM surface was measured to be 2.9 mm. Vertical distance from GM to GPA was 17.1 mm. (c) Short axis and long axis views of the GPA of five healthy subjects. The annotation in short axis imaging illustrates that the GPA depth can be quantitated via imaging. In subject 1 (long axis), the green line illustrates the ultrasound beam relative to the A-line; the yellow is the vessel angle relative to the A-line (these are both the same for all subjects). (d) Representative physiological data showing Doppler velocity as a function of time.

Results

Resolution characterization using phantoms

The axial and lateral resolution of SS-19–128 (19 MHz) was $116.5\,\mu m$ and $101.9\,\mu m$, respectively (Figure 1e and f). We also compared the resolution values to other transducers used for intraoral imaging (Fig. S2). The axial resolution of L35-16vX was $86.3\,\mu m$ (26% higher than SS-19–128) and the lateral resolution of L35-16vX was $85.2\,\mu m$ (16% higher than SS-19–128. The axial resolution of CL15-7 was $202.9\,\mu m$ (74% lower than SS-19–128) and the lateral resolution of CL15-7 was $235.5\,\mu m$ (131% lower than SS-19–128).

GPA imaging

The anatomy of the mouth and a panoramic image of a representative GPA imaging event are shown in Figure 2a and b, along with the tooth surface of the second molar (tooth #15). Real-time imaging of this scan is shown as Supplementary Video 1. In the panorama image, the features of the tooth surface, GM, PMM, hard palate, and GPA can be visualized from left to right. Here, the vertical distance from GPA to GM of the second molar was measured as 17.1 mm, which is 16% larger than the mean vertical distance from GPA

to the second molar GM ($14.7 \pm 2.9 \,\mathrm{mm}$) measured on a total of 198 maxillary plaster models in the literature.⁴⁰

Color Doppler imaging of the GPA was next done along the short and long axis in a small cohort of five subjects (Figure 2c). For subject 1, the GPA depth from the PMM was measured as 1.7 mm (Figure 2c, top left); the other subjects had similar values.

Doppler validation

The Doppler shift was converted to blood flow velocity (Figure 2d). The relationship between Doppler angle and Doppler shift was further studied by rotating the transducer on top of the radial artery (Fig. S3). The results serve as positive and negative controls to validate the spectral Doppler imaging performance of this transducer.

We next used an exercise intervention to investigate the change in blood flow and further validate this transducer. The Doppler spectrum of radial artery at rest and after exercise is shown in Fig. S4. At rest, the baseline heart rate of the subject was 78 bpm. Immediately after exercise, the heart rate was 140 bpm—79% higher than baseline. During rest, the heart rate gradually decreased to 122 bpm (after rest for 30 sec), 118 bpm (after rest for 1 min), and 107 bpm (after rest for 2 min). After two

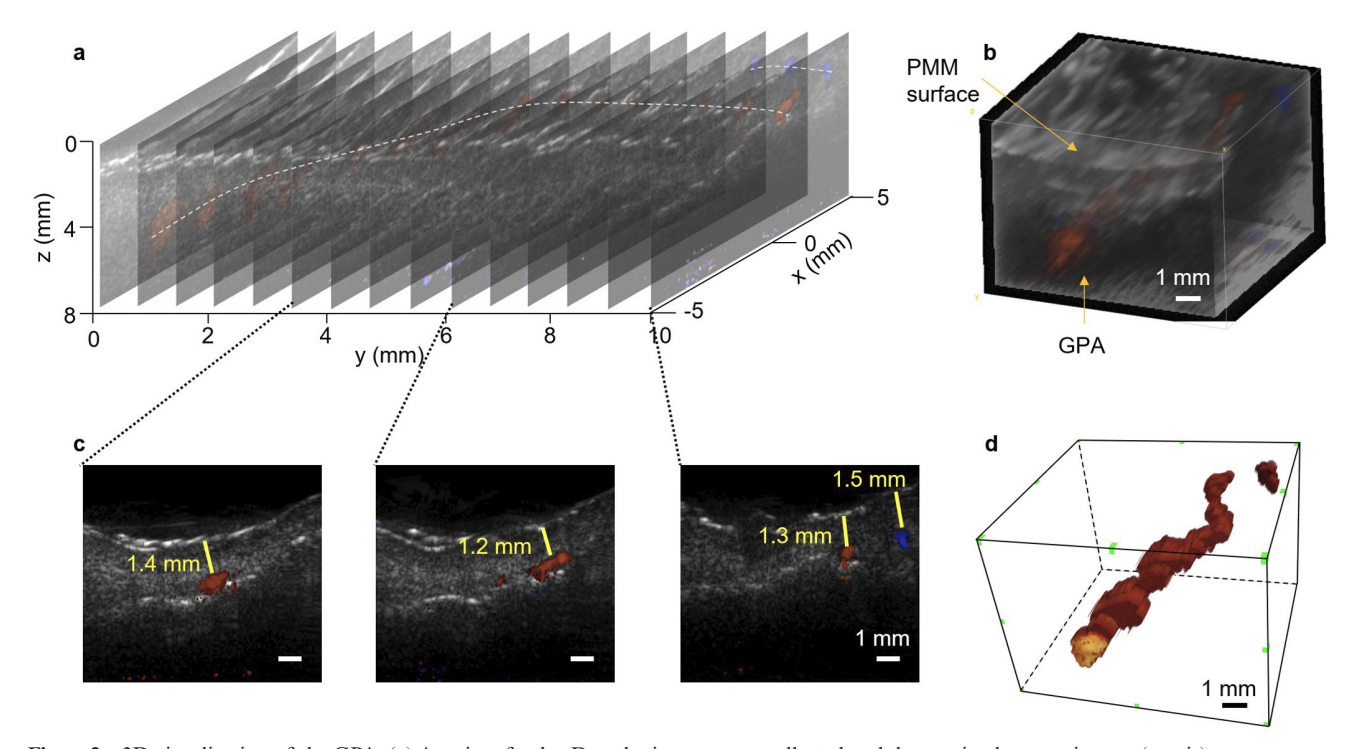


Figure 3 3D visualization of the GPA. (a) A series of color Doppler images were collected and the spacing between images (y-axis) were approximated. (b) This series could be interpolated into a 3D volumetric dataset showing the GPA and palatal masticatory mucosa (PMM). Panel (c) shows representative frames including the depth of the GPA at different locations. Panel (d) shows the trajectory of the GPA in three-dimensional similar to panel b but with only Doppler data.

minutes of rest, the heart rate returned as 137% of the baseline.

3d mapping of GPA

All 15 2D image slices and the reconstructed 3D volume image are shown in Figure 3a and b. Three representative 2D slices out of all 15 slices are shown in Figure 3c. The depth of GPA to PMM was measured as 1.4 mm, 1.2 mm, and 1.3 mm/1.5 mm for the two branches. Figure 3d shows the 3D mapping of only the GPA branches.

Full-mouth color Doppler imaging

Besides the GPA, we also imaged blood vessels in tongue (dorsal and ventral), buccal mucosa, and sublingual region on two subjects (Figure 4).

Discussion

Main findings

Most existing studies have investigated the vertical distance from GPA to GM, but failed to mention the depth of GPA from the PMM.⁴¹ Kim et al and Iwanaga et al have reported that it is critical to visualize the depth of GPA from the mucosa to assess the available thickness of palate donor and the optimal donor site for tissue grafting.^{41,42} Here, our work has shown capability

of measuring both the GPA-GM distance and the PMM thickness.

The mean dimension of posterior palate is 41 mm × 36 mm × 20 mm; the anterior palate is even smaller. Thus, the operation and movement of the bulky transducers are restricted by the teeth and cheek, causing a limited accessible imaging range of the palate. Also, the forward-facing design requires the subject to open their mouth wide to allow the transducer to reach the palate surface vertically, thus resulting in difficult positioning of the transducer. The miniaturized size with side-facing design could enable the transducer to access a large range of the palate and scan the PMM from the posterior region to the anterior region for 3D volume imaging.

The aim of the phantom study was to measure the spatial resolution of the SS-19–128 transducer and to compare it with two commercial transducers of different frequencies. The phantom study showed that the miniaturized intraoral transducer SS-19–128 has an axial resolution of 116.5 μm and a lateral resolution of 101.9 μm. According to the literature, the average distance between the GPA to the teeth increases gradually from 9.9 mm in the canine region to 13.9 mm in the second molar region, ¹⁶ while the mean thickness of the PMM is 3.8 mm. ¹⁸ These distances are 85 times and 33 times larger than the resolution of SS-19–128, respectively. In addition, the phantom study compared

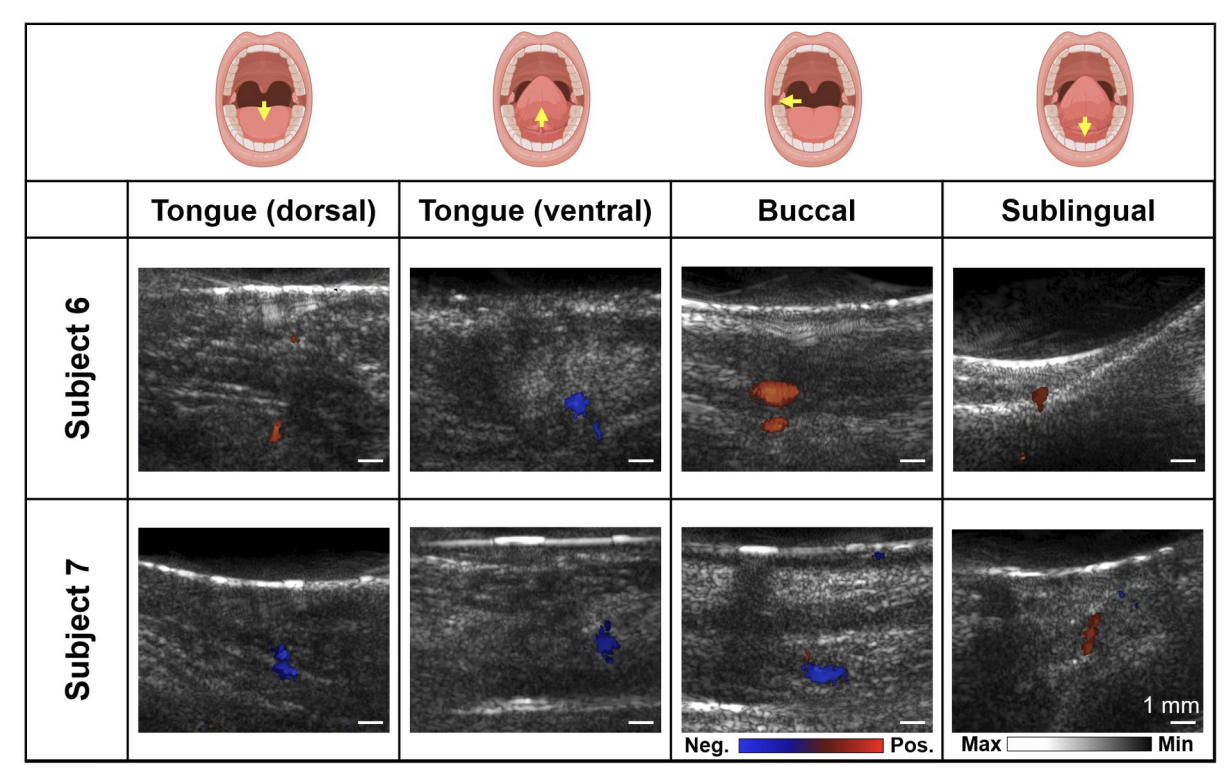


Figure 4 Imaging of the vasculature throughout the oral cavity. Yellow arrow indicates the plane represented by the color Doppler images below. Images of the vasculature at different sites of the oral cavity illustrate the ability to correlate anatomy (skin surface) with function (blood flow).

the resolution of SS-19–128 with two available commercial transducers of different frequencies in our lab. The results provide us with guidance to further improve the image quality by increasing transducer frequency. The combination of large accessible range of the palatal vault and high resolution enables the intraoral transducer to achieve high-resolution 3D imaging of the palate, from the posterior to the anterior region.

Compared to 2D imaging,³⁴ 3D imaging of the GPA from the anterior to the posterior palate is more practical for clinical applications because 3D imaging provides more intrinsic information on the volume of available palate donor for soft tissue autograft surgery⁴⁴; and 3D imaging accurately measures the trajectory of the GPA. Monnet-Corti et al suggest that during blind cutting of the palate soft tissue, the length of maximum available tissue donor was $31.7 \pm 4.0 \,\mathrm{mm}$ to avoid dissecting the GPA and causing risk of bleeding and infection.⁴⁰ Now benefiting from the 3D visualization of the GPA, surgeons could customize the regions and dimensions of the soft tissue donor for each patient.

Besides the GPA, we also imaged the color flow of the full mouth, which has been illustrated to correlate with diseases like cancer.²⁹ Due to high resolution imaging, we could detect and visualize the Doppler effects of small (~1 mm) arteries and veins inside the entire oral cavity (dorsal/ventral tongue, buccal, and sublingual regions). Doppler imaging could thus be a viable diagnostic tool for the evaluation of oral cancers such as

tongue neoplasms where pre-surgical mapping of the vasculature is needed.

Doppler can differentiate the blood flow symmetry on various sections of the tongue to diagnose the abnormalities such as tumors without perturbing the tissue.45 Moreover, studies showed that the evaluation of tongue's vascularity using intraoral Doppler imaging has a significant role in identifying predictive factors of various types of cancer, such as cervical lymph node metastasis. 46,47 Color Doppler imaging provides useful information on blood flow in oral masses not only to diagnose but also to monitor the treatment process. The decrease in blood flow in a malignant tumor after treatment/radio-chemotherapy is useful for predicting the response of a tumor to the treatment.⁴⁸ In this study, we suggest a potential role for intraoral Doppler imaging in the study of the oral mucosa, giving insights into the possibility of improving the assessment, diagnosis, and management of the conditions involving oral mucosa.

Replacing the conventional ultrasound gel with solid hydrogel improves the efficiency and reproducibility of the imaging system. Traditionally, as Lee et al reported, sufficient gel should be applied between the transducer and the PMM to obtain good-quality ultrasound images.²⁷ However, during the movement of the transducer in the oral cavity, it is common that the gel deforms due to compression. The robustness of solid hydrogel makes it keep the same shape under compression, thus the good contact between the transducer and

PMM could maintain even when the transducer moves, which provides the basis for achieving the panoramic imaging and 3D volume imaging (Fig. S5).

Limitation of the study

The vertical distance from GPA to GM of the second molar was measured to be 16% larger than the mean value measured on a total of 198 maxillary plaster models. 40 The result may be due to our current imaging process that lacks reference points, causing the scanning trajectory from the GPA to the tooth surface to not align vertically to the tooth, that is, we are imaging a curved surface with a flat transducer.

Also, although the operator tried to maintain a constant speed movement along one direction, the lack of reference points on the surface of the palatal mucosa limited the accuracy of the 3D reconstruction. Future work will mark the surface of the palate with a skin marker. By integrating the laser on the ultrasound transducer, 49,50 the markers could be measured noninvasively by photoacoustic imaging, which displays simultaneously with the ultrasound imaging, without requiring additional clinical manipulation. The 3D GPA reconstruction will thus be further improved with fiducial markers. Moreover, the distance from the GPA to teeth could be calculated by measuring the distance from reference points to teeth, which is clinically significant for evaluating the available volume of soft tissue autografting.40

The exercise intervention results demonstrate the ability of our system to detect the change of heart rate and distribution of blood flow velocity due to the intervention. We chose the radial artery for the intervention experiment because it is easier to reposition the vessel after exercise. Future work will introduce reference points for GPA imaging to improve measuring the

locations of GPA branches. Therefore, this transducer can be used to study how the GPA blood flow responds to interventions

Conclusion

In summary, we report a 3D visualization of the course of GPA and the surrounding oral anatomy. This ultrasound imaging tool can assist in the collection of soft tissue autografts by measuring the vertical distance between GPA and GM, measuring the depth from GPA to PMM, and obtaining the maximum PMM donor volume in a 3D manner.

Acknowledgment

AH and RK acknowledge federal funding from NSF2207409, and NIH under R43 DE031196. JVJ acknowledges NIH funding under R01 DE031307, R21 DE029025, and UL1 TR001442. Some figures were prepared under a license with BioRender.

Conflicts of interest

RK, AH and JVJ are co-founders of StyloSonic, LLC.

Funding

Ali Hariri and Reza Khazeinezhad acknowledge federal funding from NSF under 2207409, and NIH under R43 DE031196. Jesse V. Jokerst acknowledges NIH funding under R01 DE031307, R21 DE029025, and UL1 TR001442.

REFERENCES

- Roccuzzo M, Bunino M, Needleman I, Sanz M. Periodontal plastic surgery for treatment of localized Gingival recessions: a systematic review. *J Clin Periodontol* 2002; 178–94. https://doi.org/ 10.1034/j.1600-051x.29.s3.11.x
- 2. Sullivan HC, Atkins JH. Free Autogenous Gingival grafts. I Principles of Successful Grafting Periodontics 1968: 6: 121–29.
- Miller PD. Root coverage using the free soft tissue Autograft following Citric acid application. III. A successful and predictable procedure in areas of deep-wide recession. *Int J Periodontics Restorative Dent* 1985; 5: 14–37.
- Langer B, Langer L. Subepithelial connective tissue graft technique for root coverage. *J Periodontol* 1985; 56: 715–20. https://doi.org/10.1902/jop.1985.56.12.715
- Borghetti A, Glise JM, Monnet-Corti V, Dejou J. Comparative clinical study of a Bioabsorbable membrane and subepithelial connective tissue graft in the treatment of human Gingival recession. *J Periodontol* 1999; 70: 123–30. https://doi.org/10.1902/jop.1999.70.2.123
- Harris RJ, Miller R, Miller LH, Harris C. Complications with surgical procedures utilizing connective tissue grafts: a follow-up of 500 consecutively treated cases. *Int J Periodontics Restorative Dent* 2005; 25: 449–59.

- Tavelli L, Barootchi S, Stefanini M, Zucchelli G, Giannobile WV, Wang HL. Wound healing Dynamics, morbidity, and complications of Palatal soft-tissue harvesting. *Periodontol* 2000 2000. https://doi.org/10.1111/prd.12466
- Brasher WJ, Rees TD, Boyce WA. Complications of free grafts of Masticatory mucosa. *J Periodontol* 1975; 46: 133–38. https://doi. org/10.1902/jop.1975.46.3.133
- Tavelli L, Barootchi S, Namazi SS, Chan H-L, Brzezinski D, Danciu T, et al. The influence of Palatal harvesting technique on the donor site vascular injury: A split-mouth comparative cadaver study. J Periodontol 2020; 91: 83–92. https://doi.org/10.1002/JPER.19-0073
- Monnet-Corti V, Santini A, Glise J-M, Fouque-Deruelle C, Dillier F-L, Liébart M-F, et al. Connective tissue graft for Gingival recession treatment: assessment of the maximum graft dimensions at the Palatal vault as a donor site. *J Periodontol* 2006; 77: 899–902. https://doi.org/10.1902/jop.2006.050047
- Benninger B, Andrews K, Carter W. Clinical measurements of hard palate and implications for subepithelial connective tissue grafts with suggestions for Palatal nomenclature. *J Oral Maxillofac Surg* 2012; 70: 149–53. https://doi.org/10.1016/j.joms.2011. 03.066

- Kim D-H, Won S-Y, Bae J-H, Jung U-W, Park D-S, Kim H-J, et al. Topography of the greater Palatine artery and the Palatal vault for various types of Periodontal plastic surgery. Clin Anat 2014; 27: 578–84. https://doi.org/10.1002/ca.22252
- 13. Yu SK, Lee MH, Park BS, Jeon YH, Chung YY, Kim HJ. Topographical relationship of the greater Palatine artery and the Palatal spine. *Significance for Periodontal Surgery J Clin Periodontol* 2014; **41**: 908–13. https://doi.org/10.1111/jcpe.12288
- Reiser GM, Bruno JF, Mahan PE, Larkin LH. The subepithelial connective tissue graft Palatal donor site: anatomic considerations for Surgeons. *Int J Periodontics Restorative Dent* 1996; 16: 130–37.
- 15. Fu J-H, Hasso DG, Yeh C-Y, Leong DJM, Chan H-L, Wang H-L. The accuracy of identifying the greater Palatine neurovascular bundle: a cadaver study. *J Periodontol* 2011; **82**: 1000–1006. https://doi.org/10.1902/jop.2011.100619
- Tavelli L, Barootchi S, Ravidà A, Oh T-J, Wang H-L. What is the safety zone for Palatal soft tissue graft harvesting based on the locations of the greater Palatine artery and Foramen? A systematic review. J Oral Maxillofac Surg 2019; 77: 271. https://doi.org/ 10.1016/j.joms.2018.10.002
- Hilgenfeld T, Kästel T, Heil A, Rammelsberg P, Heiland S, Bendszus M, et al. High-resolution dental magnetic resonance imaging for planning Palatal graft surgery-a clinical pilot study. *J Clin Periodontol* 2018; 45: 462–70. https://doi.org/10.1111/jcpe. 12870
- Song J-E, Um Y-J, Kim C-S, Choi S-H, Cho K-S, Kim C-K, et al. Thickness of posterior Palatal Masticatory mucosa: the use of computerized tomography. *J Periodontol* 2008; 79: 406–12. https://doi.org/10.1902/jop.2008.070302
- Griffin TJ, Cheung WS, Zavras AI, Damoulis PD. Postoperative complications following Gingival augmentation procedures. J Periodontol 2006; 77: 2070–79. https://doi.org/10.1902/jop.2006. 050296
- Keceli HG, Aylikci BU, Koseoglu S, Dolgun A. Evaluation of Palatal donor site Haemostasis and wound healing after free Gingival graft surgery. J Clin Periodontol 2015; 42: 582–89. https:// doi.org/10.1111/jcpe.12404
- Moore CA, Law JK, Retout M, Pham CT, Chang KCJ, Chen C, et al. High-resolution Ultrasonography of Gingival biomarkers for Periodontal diagnosis in healthy and diseased subjects. *Dentomaxillofac Radiol* 2022; 51: 20220044. https://doi.org/10.1259/dmfr.20220044
- 22. Lin CY, Chen F, Hariri A, Chen CJ, Wilder-Smith P, Takesh T, et al. Photoacoustic imaging for noninvasive Periodontal probing depth measurements. *J Dent Res* 2018; **97**: 23–30. https://doi.org/10.1177/0022034517729820
- Wang X, Feng Y, Yang X, Li Z, Zhou D. Preoperative ultrasound-guided trigeminal nerve block in Orthognathic surgery: A prospective study about its efficacy of intraoperative anesthetic dosage and postoperative analgesia. *J Oral Maxillofac Surg* 2021; 79: 2042–50. https://doi.org/10.1016/j.joms. 2021.04.011
- Chan H-L, Kripfgans OD. Dental Ultrasound in Periodontology and Implantology. In: *Dental Ultrasound in Periodontology and Implantology*. Cham: Springer; 2021., pp. 161–75. https://doi.org/10.1007/978-3-030-51288-0
- Betancourt AR, Samal A, Chan H-L, Kripfgans OD. Overview of ultrasound in dentistry for advancing research methodology and patient care quality with emphasis on Periodontal/peri-implant applications. Zeitschrift Für Medizinische Physik 2023.
- Sampietro-Martínez R, Pérez-Monreal J, Sánchez-Torres A, Bara-Casaus J, Gay-Escoda C. Color Doppler ultrasound for the assessment of Palatal Fibromucosa thickness and the trajectory of the greater Palatine artery: A pilot study. *J Clin Exp Dent* 2022; 14: e528–33. https://doi.org/10.4317/jced.59704
- Lee KH, Park W, Cheong J, Park KM, Kim JW, Kim KD. Identifying the course of the greater Palatine artery using Intraoral Ultrasonography: cohort study. Surg Radiol Anat 2022; 44: 1139–46. https://doi.org/10.1007/s00276-022-02967-y
- Zucchelli G, Mounssif I. Periodontal plastic surgery. Periodontol 2000 2015; 68: 333–68. https://doi.org/10.1111/prd.12059

- Yoon BC, Bulbul MD, Sadow PM, Faquin WC, Curtin HD, Varvares MA, et al. Comparison of intraoperative Sonography and histopathologic evaluation of tumor thickness and depth of invasion in oral tongue cancer: A pilot study. AJNR Am J Neuroradiol 2020; 41: 1245–50. https://doi.org/10.3174/ajnr.A6625
- Qi B, Hariri A, Khazaeinezhad R, Fu L, Li Y, Jin Z, et al. A Miniaturized ultrasound transducer for monitoring full-mouth oral health: a preliminary study. *Dentomaxillofac Radiol* 2023; 52: 20220220. https://doi.org/10.1259/dmfr.20220220
- Rossmann K. Point spread-function, line spread-function, and modulation transfer function: tools for the study of imaging systems. *Radiology* 1969; 93: 257–72. https://doi.org/10.1148/93. 2.257
- Fu L, Ling C, Jin Z, Luo J, Palma-Chavez J, Wu Z, et al. Photoacoustic imaging of posterior Periodontal pocket using a commercial hockey-stick transducer. *J Biomed Opt* 2022; 27(5): 056005. https://doi.org/10.1117/1.JBO.27.5.056005
- 33. He T, Bradley DG, Xu M, Ko S-T, Qi B, Li Y, et al. Bio-inspired Degradable Polyethylenimine/calcium phosphate Micro-/Nanocomposites for transient ultrasound and photoluminescence imaging. *Chem Mater* 2022; 34: 7220–31. https://doi.org/10.1021/acs.chemmater.2c00857
- Sampietro-Martínez R, Pérez-Monreal J, Sánchez-Torres A, Bara-Casaus J, Gay-Escoda C. Color Doppler ultrasound for the assessment of Palatal Fibromucosa thickness and the trajectory of the greater Palatine artery: A pilot study. J Clin Exp Dent 2022; 14: e528–33. https://doi.org/10.4317/jced.59704
- Wang C, Qi B, Lin M, Zhang Z, Makihata M, Liu B, et al. Continuous monitoring of deep-tissue Haemodynamics with Stretchable ultrasonic phased arrays. *Nat Biomed Eng* 2021; 5: 749–58. https://doi.org/10.1038/s41551-021-00763-4
- Sun J-Y, Zhao X, Illeperuma WRK, Chaudhuri O, Oh KH, Mooney DJ, et al. Highly Stretchable and tough Hydrogels. Nature 2012; 489: 133–36. https://doi.org/10.1038/nature11409
- 37. Yang CH, Wang MX, Haider H, Yang JH, Sun J-Y, Chen YM, et al. Strengthening Alginate/Polyacrylamide Hydrogels using various multivalent Cations. *ACS Appl Mater Interfaces* 2013; 5: 10418–22. https://doi.org/10.1021/am403966x
- 38. Stalling D, Westerhoff M, Hege H-C. Amira: a highly interactive system for visual data analysis. In: *The Visualization Handbook*.; 2005, pp. 749–67.
- Schneider CA, Rasband WS, Eliceiri KW. NIH image to Imagej: 25 years of image analysis. *Nat Methods* 2012; 9: 671–75. https://doi.org/10.1038/nmeth.2089
- Monnet-Corti V, Santini A, Glise J-M, Fouque-Deruelle C, Dillier F-L, Liébart M-F, et al. Connective tissue graft for Gingival recession treatment: assessment of the maximum graft dimensions at the Palatal vault as a donor site. *J Periodontol* 2006; 77: 899–902. https://doi.org/10.1902/jop.2006.050047
- Kim D-H, Won S-Y, Bae J-H, Jung U-W, Park D-S, Kim H-J, et al. Topography of the greater Palatine artery and the Palatal vault for various types of Periodontal plastic surgery. *Clin Anat* 2014; 27: 578–84. https://doi.org/10.1002/ca.22252
- 42. Iwanaga J, Tanaka T, Ibaragi S, Okui T, Hamaguchi J, Min S, et al. Revisiting major anatomical risk factors of Maxillary sinus lift and soft tissue graft harvesting for dental implant Surgeons. Surg Radiol Anat 2020; 42: 1025–31. https://doi.org/10.1007/s00276-020-02468-w
- M Ahmad Z. Palatal dimensions and its correlation with the circumference of upper anterior teeth. *RDENTJ* 2009; 9: 259–67. https://doi.org/10.33899/rden.2009.9124
- 44. Kuriakose A, Raju S. Assessment of thickness of Palatal Mucosal donor site and its association with age and gender. *J Indian Soc Periodontol* 2012; **16**: 370–74. https://doi.org/10.4103/0972-124X. 100913
- Kimura Y, Ariji Y, Gotoh M, Toyoda T, Kato M, Kawamata A, et al. Doppler Sonography of the deep lingual artery. *Acta Radiol* 2001; 42: 306–11. https://doi.org/10.1080/028418501127346693
- 46. Ariji Y, Goto M, Fukano H, Sugita Y, Izumi M, Ariji E. Role of Intraoral color Doppler Sonography in predicting delayed Cervical lymph node metastasis in patients with early-stage tongue cancer: a

- pilot study. Oral Surg Oral Med Oral Pathol Oral Radiol 2015; 119: 246–53. https://doi.org/10.1016/j.oooo.2014.10.021
- 47. Yamamoto C, Yuasa K, Okamura K, Shiraishi T, Miwa K. Vascularity as assessed by Doppler Intraoral ultrasound around the invasion front of tongue cancer is a Predictor of pathological grade of malignancy and Cervical lymph node metastasis. Dentomaxillofac Radiol 2016; **45**: 20150372. https://doi.org/10.1259/ dmfr.20150372
- 48. Gandhi R, Bhowate R, Navyar AS, Gandhi S, Dongarwar G. Color Doppler-Ultrasonography in oral squamous cell carcinoma:
- making Ultrasonography more meaningful. Adv Biomed Res
- 2016; **5**: 29. https://doi.org/10.4103/2277-9175.178068 49. Fu L, Khazaeinezhad R, Hariri A, Qi B, Chen C, Jokerst JV. Posterior Photoacoustic/ultrasound imaging of the Periodontal pocket with a compact Intraoral transducer. Photoacoustics 2022; 28: 100408. https://doi.org/10.1016/j.pacs.2022.100408
- 50. Yim W, Zhou J, Sasi L, Zhao J, Yeung J, Cheng Y, et al. 3d-Bioprinted phantom with human skin Phototypes for BIOMED-ICAL optics. Adv Mater 2023; 35: e2206385. https://doi.org/10. 1002/adma.202206385